Morphotropism in fumarolic mineral-related anhydrous sulfates: novel representatives in A + 2 M 2+(SO4)2 and A + 2 M 2+ 2(SO4)3 series

Oleg I Siidra, Diana Nekrasova, Olga Blatova, Marie Colmont, Olivier Mentré, Dmitri Charkin

Morphotropism in fumarolic mineral-related anhydrous sulfates: novel representatives in $A^+_2M^{2+}(SO_4)_2$ and $A^+_2M^{2+}_2(SO_4)_3$ series

Oleg I. Siidra,[a,b]* Diana Nekrasova,[a,c] Olga Blatova,[d] Marie Colmont,[c] Olivier Mentré[c] and Dmitri Charkin[e]

[a]Department of Crystallography, St. Petersburg State University, University emb. 7/9, 199034 Saint-Peterburg, Russian Federation, [b]Kola Science Center, Russian Academy of Sciences, Apatity, Murmansk Region, 184200, Russian Federation, [c]Université Lille, CNRS, Centrale Lille, Université Artois, UMR 8181, Unité de Catalyse et Chimie du Solide, Lille, F-59000, France, [d]Samara State Technical University, Molodogvardeyskaya st. 244, Samara 443100, Russian Federation, and [e]Department of Chemistry, Moscow State University, Leninskie Gory 1, 119991, Russian Federation. *Correspondence e-mail: o.siidra@spbu.ru

The discovery of numerous endemic anhydrous sulfate minerals in fumaroles of the Tolbachik volcano (Kamchatka, Russia) has revived interest in the whole family of anhydrous sulfates. Herein is reported the crystal structure of $Cs_2Cu(SO_4)_2$ which adds important data on the 'final' contributor with the largest A^+ cation to the $A_2[Cu(SO_4)_2]$ morphotropic series (A = Na, K, Rb, Cs), the 'initial' structurally characterized representative of this family being saranchinaite $Na_2Cu(SO_4)_2$. With increasing ionic radius of the alkali metal cation(s), embedded in the $[Cu(SO_4)_2]^{2-}$ framework, symmetry-breaking transformations occur. $Cs_2Cu(SO_4)_2$, which is here designated as the ε-phase, has a layered structure. $Cs_2Co_2(SO_4)_3$ is a new representative of another morphotropic series of the orthorhombic $A_2[M^{2+}_2(SO_4)_3]$ family, being also the first anhydrous Cs–Co sulfate. Structural relationships in $A^+_2M^{2+}(SO_4)_2$ and $A^+_2M^{2+}_2(SO_4)_3$ morphotropic series are discussed in detail.

1. Introduction

Until recently, anhydrous sulfates of alkali and transition metals were a blank spot in the crystal chemistry of sulfates, not the least due to their low stability in humid air (Siidra *et al.*, 2021*a*). In the meantime, hydrated sulfate species are represented widely both among synthetic compounds and minerals (Hawthorne *et al.*, 2000). In the last decade, high-temperature fumaroles with strongly oxidizing conditions on the Tolbachik volcano (Kamchatka, Russia) (Vergasova & Filatov, 2012) produced an amazingly large number of new mineral species, including anhydrous sulfates, whereof a large part correspond to their own, new structure types (*e.g.* Siidra *et al.*, 2018*a*,*b*; Filatov *et al.*, 2020; Zubkova *et al.*, 2021), with no synthetic analogs known (Siidra *et al.*, 2017, 2020*a*). Of particular interest are the anhydrous copper sulfates bearing rare elements, *e.g.* caesium (Pekov *et al.*, 2018). Our recent studies revealed the existence of several synthetic analogs for some of these minerals (Nekrasova *et al.*, 2021*a*), including compounds of another rare alkali metal, rubidium (Nekrasova *et al.*, 2021*b*; Siidra *et al.*, 2021*b*, see also references therein). Magnetic (Nekrasova *et al.*, 2020) and electrochemical (Kovrugin *et al.*, 2019) studies made on single-phase synthetic analogs have shown some of them to exhibit interesting properties. It is worth noting that most known alkali copper sulfate representatives are structurally based on three-dimensional copper sulfate frameworks (Borisov *et al.*, 2021).

While several examples of Rb–Cu sulfates have been recently reported (Siidra *et al.*, 2021*a*), anhydrous sulfates of caesium with copper, as well as with cobalt, remain mostly unaddressed; to the best of our knowledge, no reliable data have been reported. In order to fill this gap and to elucidate the effect of alkali cation size on the structural architectures of two relatively numerous series, $A^{I}_2Cu(SO_4)_2$ and $A^{I}_2M^{II}_2(SO_4)_3$, we have undertaken this study.

2. Experimental

2.1. Synthesis

Single crystals of $Cs_2Cu(SO_4)_2$ were synthesized by solid-state reactions under vacuum using a mixture of Cs_2SO_4 (Alfa Aesar, 99%), $CuSO_4$ (Prolabo, 98%) and CuO (Prolabo, 98%) in 1:2:2 ratio. $CuSO_4$ was pre-dried at 673 K for 12 h and further ground with Cs_2SO_4 and CuO in an agate mortar in air for 10 min. The mixture was pressed into a pellet (~5 mm × 2 mm) and loaded into a silica ampoule (~10 cm × 0.8 cm), which was evacuated (10^{-2} mbar) and further sealed. The ampoule was heated up to 973 K for 3 h and kept for 10 h. Cooling to 773 K was performed over 96 h, and an extra 12 h to room temperature. The products consisted of dark blue crystals of $Cs_2Cu(SO_4)_2$, sky-blue crystals of $Cs_2Cu_3(SO_4)_4$ (Fig. 1) and green crystals of $Cs_2Cu_{3.5}O_{1.5}(SO_4)_3$ (Nekrasova *et al.*, 2021*b*).

Crystals of $Cs_2Co_2(SO_4)_3$ were obtained under a similar synthetic protocol. Cs_2SO_4 (Sigma-Aldrich, 99.99%) and $CoSO_4$ (Prolabo, 98%) were mixed carefully in an agate mortar in ratio 1:3, pelletized, sealed and annealed as described above. The product consisted of violet $Cs_2Co_2(SO_4)_3$ crystals.

2.2. X-ray experiment

Crystals of the new compounds were mounted on glass fibers and studied on a Bruker APEX II DUO X-ray diffractometer equipped with a micro-focus X-ray tube (Ag $K\alpha$ radiation, 50 kV, 0.6 mA). The data were integrated and corrected for absorption using a multiscan-type model implemented in the programs *APEX* and *SADABS* (Bruker, 2014). More than a hemisphere of X-ray diffraction data were collected. Both structures were solved by direct methods and refined using the *SHELX* software package (Sheldrick, 2015). Crystallographic data are given in Table 1. For $Cs_2Co_2(SO_4)_3$, the $|E^2 - 1|$ parameter was 0.724 which clearly indicated a high probability of non-centrosymmetric (NCS) structure (Marsh, 1995) further confirmed by structure solution and refinement. In both structures, atomic displacement parameters of all atoms were refined anisotropically. Selected interatomic distances are given in Table 2. The bond-valence sums for the atoms in both structures were calculated using parameters given by Gagné & Hawthorne (2015) for Cu^{2+}—O, Co^{2+}—O, Cs^{+}—O and S^{6+}—O bonds. The results are summarized in Tables 3 and 4. The bond-valence sums for all atoms are in a good agreement with their formal valences.

Table 1
Crystallographic data and refinement parameters.

Experiments were carried out at 296 K.

	$Cs_2Cu(SO_4)_2$	$Cs_2Co_2(SO_4)_3$
Space group	$P2_1/n$	$P2_12_12_1$
a (Å)	9.685 (3)	4.8810 (7)
b (Å)	7.920 (3)	14.920 (2)
c (Å)	12.141 (4)	17.164 (3)
β (°)	91.416 (8)	
V (Å^3)	931.0 (5)	1249.9 (3)
D_x (g cm^{-3})	3.721	3.570
Crystal size (mm)	0.20 × 0.20 × 0.15	0.10 × 0.15 × 0.15
θ max (°)	26.344	25.198
No. total reflections collected	16754	13460
Unique reflections, R_{int}	3770, 0.07	4542, 0.08
Unique reflections $F > 4\sigma(F)$	2389	2909
R_1	0.042	0.049
wR_1	0.085	0.060
S	1.011	0.991
ρ_{max}, ρ_{min} (e Å^{-3})	1.434, −1.768	1.501, −1.324
CCDC No.	2103648	2104096

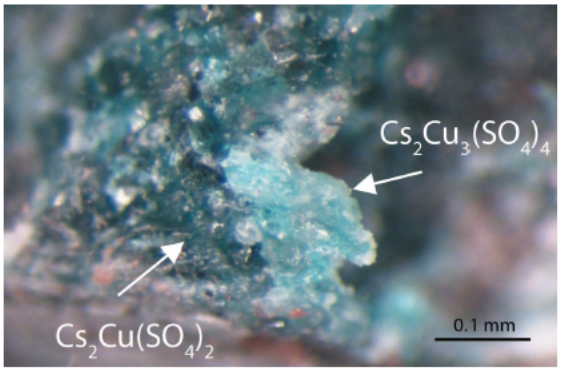

Figure 1
Crystalline aggregates of $Cs_2Cu(SO_4)_2$ and $Cs_2Cu_3(SO_4)_4$ viewed under an optical microscope.

2.3. Topological analysis

Topological analysis was performed using the *TopoPro* (Blatov *et al.*, 2014) program package. All crystal structures were simplified according to the common protocol of omitting the alkali cations and squeezing the sulfate tetrahedra into their mass centers. The resulting nets describe the connectivity (topology) of the complex polymeric groups comprised of copper or cobalt cations and sulfate anions. These underlying nets were assigned to topological types by computing their topological indices and comparing them to the reference values from the *TopoPro* TTD collection (Blatov *et al.*, 2014). Common building units for the different phases were found with hierarchical generation of subnets of the underlying nets by enumeration of all ways of breaking net edges (Blatov, 2006).

Table 2
Selected interatomic distances (Å) in the structure of $Cs_2Cu(SO_4)_2$ and $Cs_2Co_2(SO_4)_3$.

$Cs_2Cu(SO_4)_2$				$Cs_2Co_2(SO_4)_3$			
Cs1—O5	2.985 (4)	Cu1—O3	1.919 (4)	Cs1—O6	2.991 (7)	Co1—O8	1.994 (7)
Cs1—O7	3.096 (6)	Cu1—O1	1.986 (4)	Cs1—O3	3.095 (8)	Co1—O2	2.002 (7)
Cs1—O7	3.170 (5)	Cu1—O6	2.003 (4)	Cs1—O1	3.114 (7)	Co1—O4	2.017 (6)
Cs1—O1	3.194 (4)	Cu1—O2	2.019 (4)	Cs1—O5	3.127 (7)	Co1—O11	2.095 (7)
Cs1—O6	3.250 (5)	Cu1—O8	2.195 (4)	Cs1—O6	3.241 (8)	Co1—O9	2.120 (7)
Cs1—O2	3.263 (4)	Cu1···S2	2.5837 (16)	Cs1—O8	3.295 (8)		
Cs1—O4	3.469 (5)			Cs1—O1	3.304 (7)	Co2—O10	1.948 (7)
Cs1—O5	3.504 (4)	S1—O4	1.441 (4)	Cs1—O9	3.331 (8)	Co2—O12	1.956 (7)
Cs1—O2	3.532 (5)	S1—O5	1.448 (4)	Cs1—O6	3.368 (8)	Co2—O5	1.973 (7)
Cs1—O8	3.679 (7)	S1—O3	1.492 (4)	Cs1—O2	3.431 (8)	Co2—O3	1.992 (7)
Cs1—O8	3.691 (7)	S1—O1	1.504 (4)	Cs1—O5	3.772 (7)	Co2—O7	2.689 (7)
		⟨S1—O⟩	1.471				
Cs2—O4	3.008 (4)			Cs2—O7	3.121 (8)	S1—O1	1.448 (6)
Cs2—O3	3.029 (4)	S2—O8	1.434 (4)	Cs2—O11	3.141 (8)	S1—O9	1.463 (7)
Cs2—O5	3.187 (4)	S2—O7	1.446 (5)	Cs2—O7	3.188 (8)	S1—O2	1.480 (7)
Cs2—O6	3.286 (4)	S2—O2	1.495 (4)	Cs2—O12	3.203 (7)	S1—O12	1.484 (7)
Cs2—O8	3.310 (6)	S2—O6	1.495 (5)	Cs2—O4	3.236 (7)	⟨S1—O⟩	1.469
Cs2—O7	3.323 (5)	⟨S2—O⟩	1.468	Cs2—O10	3.316 (8)		
Cs2—O1	3.383 (4)			Cs2—O1	3.431 (7)	S2—O6	1.444 (7)
Cs2—O4	3.411 (5)			Cs2—O4	3.462 (7)	S2—O11	1.464 (7)
Cs2—O2	3.584 (4)			Cs2—O1	3.514 (7)	S2—O8	1.488 (6)
Cs2—O6	3.721 (5)			Cs2—O2	3.550 (8)	S2—O5	1.493 (7)
				Cs2—O12	3.781 (8)	⟨S2—O⟩	1.472
						S3—O7	1.447 (8)
						S3—O10	1.464 (6)
						S3—O4	1.474 (6)
						S3—O3	1.486 (8)
						⟨S3—O⟩	1.468

Table 3
Bond–valence values (expressed in valence units) for $Cs_2Cu(SO_4)_2$.

	O1	O2	O3	O4	O5	O6	O7	O8	$\Sigma_i a$
Cs1	0.11	0.10		0.06	0.19	0.10	0.14	0.03	0.98
		0.05		0.05			0.12	0.03	
Cs2	0.07	0.04	0.17	0.18	0.11	0.09	0.08	0.08	0.92
				0.07		0.03			
Cu1	0.43	0.39	0.52			0.41		0.24	1.99
S1	1.39		1.43	1.62	1.59				6.03
S2		1.42				1.42	1.60	1.65	6.09

Table 4
Bond–valence values (expressed in valence units) for $Cs_2Co_2(SO_4)_3$.

	O1	O2	O3	O4	O5	O6	O7	O8	O9	O10	O11	O12	$\Sigma_i a$
Cs1	0.14	0.06	0.14		0.13	0.18		0.09	0.08				1.11
	0.09				0.03	0.10							
						0.07							
Cs2	0.06	0.05		0.10			0.13	0.08			0.13	0.11	0.91
	0.05			0.06			0.11					0.03	
Co1		0.45		0.43				0.46	0.33		0.35		2.02
Co2			0.46		0.48		0.07			0.51		0.50	2.02
S1	1.59	1.47							1.54			1.46	6.06
S2					1.42	1.61		1.44			1.53		6.00
S3			1.45	1.49			1.60			1.53			6.07
$\Sigma_v c$	1.93	2.03	2.05	2.08	2.06	1.96	1.91	2.07	1.95	2.04	2.01	2.1	

3. Results

3.1. $Cs_2Cu(SO_4)_2$

The structure of $Cs_2Cu(SO_4)_2$ features two symmetry-independent Cs^+ cations. Taking the maximal value of the Cs—O bond lengths as 3.80 Å, Cs1 site can be described as eleven-coordinate, while Cs2, as ten-coordinate, with Cs–O separations ranging from 2.985 (4) to 3.721 (5) Å (Table 2).

The Cu1 atom forms four short and strong $Cu—O_{eq}$ bonds (≤2 Å) forming a somewhat distorted CuO_4 plane square which is complemented by a fifth longer $Cu—O_{ap}$ bond of 2.195 (4) Å, to yield the typical CuO_5 moiety (Fig. 2). According to Burns & Hawthorne (1995), this coordination can be described as intermediate from square pyramidal to triangular bipyramidal. All Cu—O bonds ≤3.05 Å were taken

into consideration. Note the presence of a very short Cu1–S2 distance of 2.5837 (16) Å arising from the relatively rare bidentate (κ^2)-coordination of the sulfate $S2O_4^{2-}$ tetrahedron to the $Cu1^{2+}O_5$ polyhedron.

There are two symmetry-independent S^{6+} cations in the structure, each tetrahedrally coordinated by four O atoms with the average ⟨S—O⟩ bond length of 1.47 Å which agrees with the common mean value for sulfates (Hawthorne *et al.*, 2000).

The Cu-centered CuO_5 polyhedra and SO_4 tetrahedra form $[Cu(SO_4)_2]^{2-}$ layers with large voids depicted in Fig. 3. The Cs^+ cations are located in the interlayer space 'below' and 'above' these voids [Figs. 4(*a*) and 4(*b*)]. The edge sharing between the CuO_5 polyhedra and $S2O_4$ tetrahedra is a unique structural feature of $Cs_2Cu(SO_4)_2$. Edge sharing between CuO_n polyhedra and SO_4 tetrahedra is rare and has been hitherto described only for CuO_6 octahedra in anhydrous sulfates only (Cu–S distances are given in brackets): chlorothionite, $K_2CuCl_2(SO_4)$ [2.593 (2) Å] (Giacovazzo *et al.*, 1976), $Rb_2Cu(SO_4)_2$ [2.572 (2) Å] and several other Rb–Cu sulfates (Siidra *et al.*, 2021*b*) and $KNaCu(SO_4)_2$ [2.810 (2) Å] (Borisov *et al.*, 2021). The structure of $Cs_2Cu(SO_4)_2$ is therefore the first example of such coordination involving CuO_5 species. This bidentate (κ^2)-coordination of sulfate anion to another metal cation (*i.e.* the edge sharing) has been recently observed in the complex Zn sulfate majzlanite, $K_2Na(ZnNa)Ca(SO_4)_4$ (Siidra *et al.*, 2020), where the Zn–S distance is 2.870 (2) Å.

3.2. $Cs_2Co_2(SO_4)_3$

This structure also contains two Cs^+ sites both of which are eleven-coordinate (Fig. 5). The coordination of Cs^+ cations is similar in $Cs_2Co_2(SO_4)_3$ and $Cs_2Cu(SO_4)_2$.

In contrast, the two Co sites have different coordination (Table 2). The Co1 centers a rather uncommon CoO_5 trigonal bipyramid. The Co1—O8, Co1—O2, and Co1—O4 bonds, with separations of ~2.0 Å, form a just slightly corrugated equatorial plane while longer Co1—O11 and Co1—O9 bonds constitute the corresponding axis. Co2 atoms form four short and strong bonds in the range of 1.948 (7)–1.992 (7) Å forming a CoO_4 tetrahedron complemented by a fifth long Co2—O7 bond of 2.689 (7) Å. This $Co2O_5$ [4+1] coordination can be described as transitional from tetrahedral to trigonal bipyramidal, akin to Cu1 in $Cs_2Cu(SO_4)_2$. While Co^{2+}, in contrast to Cu^{2+}, more commonly adopts an octahedral environment, the Jahn–Teller effect for a high-spin 3*d* configuration effectively makes the coordination sphere of Co^{2+} rather flexible.

The three symmetry-independent sulfate groups in the structure of $Cs_2Co_2(SO_4)_3$ are relatively regular with an

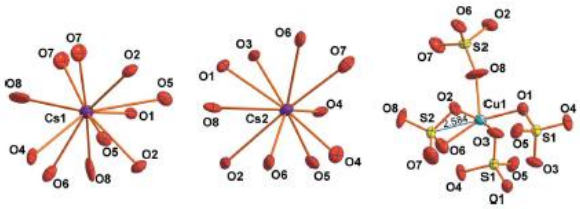

Figure 2
Coordination of atoms in the structure of $Cs_2Cu(SO_4)_2$. Displacement ellipsoids are drawn at the 50% probability level. Distance given in Å.

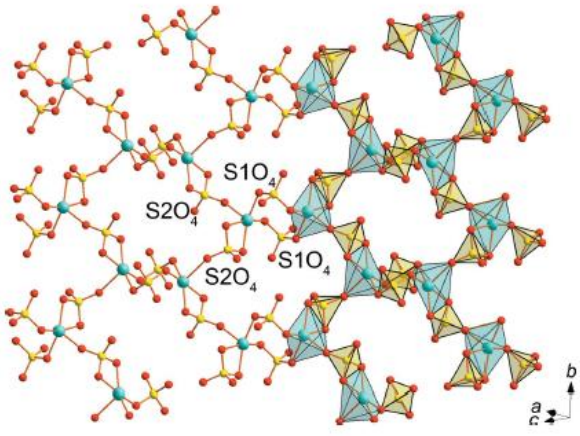

Figure 3
$Cu(SO_4)_2]^{2-}$ layer in the structure of $Cs_2Cu(SO_4)_2$ (CuO_5 in blue, SO_4 in yellow).

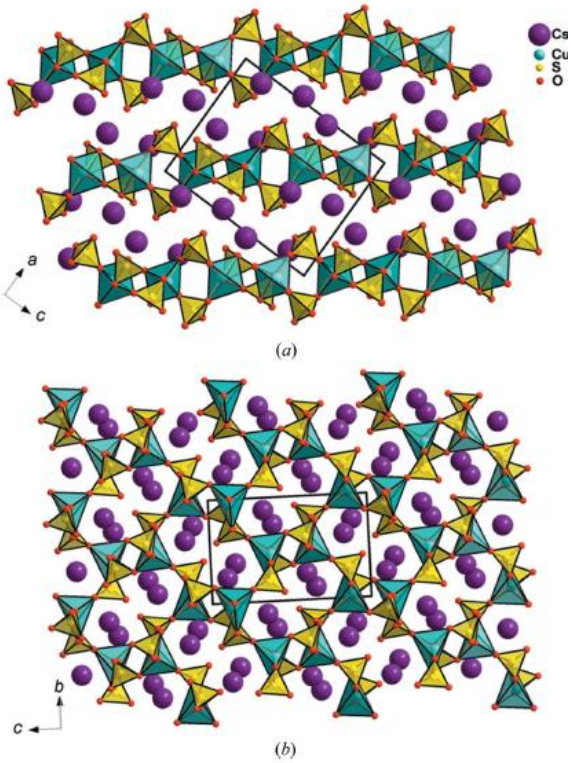

Figure 4
General projections of the crystal structure of $Cs_2Cu(SO_4)_2$ (*a*) along **b** and (*b*) along **a**. Cs–O bonds are not shown for clarity.

average ⟨S—O⟩ bond length of 1.47 Å, again in very good agreement with the overall average distance of 1.473 Å given for sulfate minerals by Hawthorne *et al.* (2000).

In general, the structural topology of the layer in $Cs_2Co_2(SO_4)_3$ exhibits much in common to that of $Cs_2Cu(SO_4)_2$. The interconnection of Co-centered polyhedra with sulfate tetrahedra occurs via common vertices as well as via common edges with the formation of $[Co_2(SO_4)_3]^{2-}$ corrugated layers with elliptical large cavities [Fig. 6(*a*)]. This layered structural topology is the result of the adaptation of cobalt sulfate species to the large caesium cations in the interlayer [Fig. 6(*b*)].

4. Discussion

Both new compounds have no structural analogs to date and add new members and new structure types to the family of anhydrous alkali transition metal sulfates.

4.1. $Cs_2Cu(SO_4)_2$

To date, there is an only representative, the Tutton-like caesium copper sulfate hexahydrate, $Cs_2[Cu(H_2O)_6](SO_4)_2$ (Ballirano *et al.*, 2007), whose identity has been unambiguously proved. Nagase *et al.* (1978) studied its thermal decomposition but only via TGA runs whence they deduced formation of a monohydrate or hemihydrate transient [$\sim 0.7H_2O$ per $Cs_2Cu(SO_4)_2$ formula unit] which totally dehydrated at 505 K. There are also two thermal effects at 686 K and 772 K which were attributed to phase transition and melting but no X-ray data were provided, except the noted crystallinity over the temperature range. The lack of chemical identity of the compounds formed does not, as yet, rule out various side processes like partial hydrolysis in the open system which explains the non-integer hydration number calculated from the DTA data. Two unindexed XRD patterns claimed to correspond to two polymorphs of $Cs_2Cu(SO_4)_2$ were provided by Tardy *et al.* (1972). Foret *et al.* (1982) and later Papánková *et al.* (1985) reported a series of unindexed powder patterns for the dehydration products of the double $A_2Cu(SO_4)_2{\cdot}nH_2O$ copper sulfates (A = Na, n = 2; A = K, Rb, Tl, Cs, n = 6) along with IR spectroscopy data. From those they concluded that the anhydrous $A_2Cu(SO_4)_2$ compounds are not isostructural and the binding modes of sulfate groups to the copper cations are also different. Qualitatively, these conclusions were correct; we note however that the published unindexed XRD patterns correspond neither to each other nor to the calculated powder pattern of $Cs_2Cu(SO_4)_2$ described here. As yet, the chemistry of anhydrous Cs–Cu (oxo)sulfates remains at the early stage of development so further studies are evidently necessary to resolve these contradictions and fully interpret the results of Tardy *et al.* (1972), Foret *et al.* (1982) and Papánková *et al.* (1985) which suggest the existence of a variety of yet unidentified new species. We also note that our crystals of $Cs_2Cu(SO_4)_2$ were obtained by cooling the melt from a temperature (~473 K) well above the reported melting point and they most likely correspond to the high-temperature polymorph; the chemistry of the polymorphs and water-poor species remains undeveloped.

The determination of the crystal structure of $Cs_2Cu(SO_4)_2$ provides the data for the 'final' contributor with the largest A^+ cation to the $A_2Cu(SO_4)_2$ series (A = Na, K, Rb, Cs) listed in Table 5 and illustrated in Fig. 7. The first 'initial' structurally characterized representative of this family was saranchinaite $Na_2Cu(SO_4)_2$ (Siidra *et al.*, 2018*a*), discovered in 2015 (proposal IMA 2015-019). Before its discovery the structural features of the $A_2Cu(SO_4)_2$ compounds were totally obscure. Surprisingly, attempts to determine the structural features of the product of kröhnkite $Na_2Cu(SO_4)_2(H_2O)_2$ dehydration, first reported by Nagase *et al.* (1978), continued for many decades [see *e.g.* Testasicca *et al.* (2016)] but with little success. During the last three years, we have found that $A_2Cu(SO_4)_2$ (A = Na, K, Rb) compounds constitute a complex morphotropic series which consists of at least five different structural modifications [α-, β-, γ- and δ-phases, see Siidra *et al.* (2021*a*)]. This work completes the structural series from the large-cation side adding the ε-type for A = Cs (Table 5). With increasing

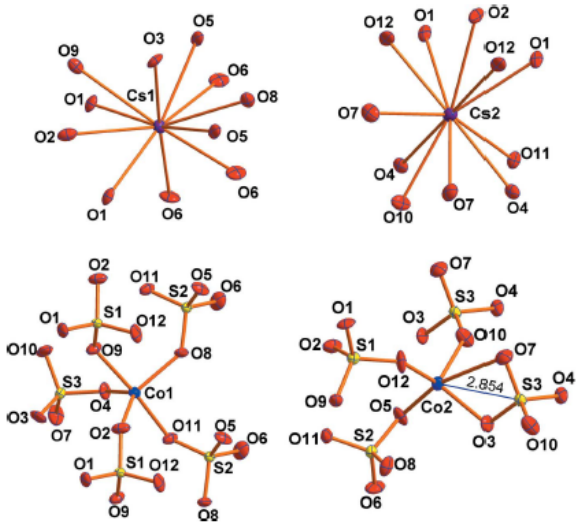

Figure 5
Coordination of atoms in the structure of $Cs_2Co_2(SO_4)_3$. Displacement ellipsoids are drawn at the 50% probability level.

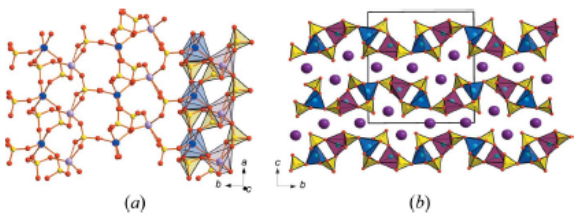

Figure 6
(*a*) $Co_2(SO_4)_3]^{2-}$ layer in the structure of $Cs_2Co_2(SO_4)_3$. ($Co1O_5$ = blue, $Co2O_5$ = lilac). (*b*) General projection of the crystal structure of $Cs_2Co_2(SO_4)_3$. Cs—O bonds are not shown for clarity.

Table 5
Crystallographic parameters of known saranchinaite morphotropic series $A_2[Cu(SO_4)_2]$ compounds.

Phase modification	α-phase		β-phase	γ-phase				δ-phase	ε-phase
Mineral	Saranchinaite	Synthetic	Synthetic	Synthetic	Synthetic	Synthetic	Synthetic	Synthetic	Synthetic
Synthetic formula	$Na_2[Cu(SO_4)_2]$	$Na_2[Cu(SO_4)_2]$	$K(Na,K)Na_2[Cu_2(SO_4)_4]$	$KNa[Cu(SO_4)_2]$	$K_2[Cu_2(SO_4)_2]$	$RbNa[Cu(SO_4)_2]$	$RbK[Cu(SO_4)_2]$	$Rb_2[Cu(SO_4)_2]$	$Cs_2[Cu(SO_4)_2]$
Space group	$P2_1$	$P2_1$	$P2_1/c$	$C2/c$	$C2/c$	$C2/c$	$C2/c$	$Pna2_1$	$P2_1/n$
a (Å)	9.0109 (5)	8.9711 (3)	12.5085 (9)	15.9721 (10)	16.0433 (11)	16.034 (3)	16.1865 (14)	9.2521 (4)	9.685 (3)
b (Å)	15.6355 (8)	15.5482 (5)	9.3166 (7)	9.4576 (6)	9.7819 (7)	9.560 (2)	10.0026 (9)	10.9671 (5)	7.920 (3)
c (Å)	10.1507 (5)	10.1421 (3)	12.7894 (10)	9.0679 (6)	9.2341 (7)	9.170 (2)	9.3923(8	8.9612 (4)	12.141 (4)
β (°)	107.079 (2)	107.155 (1)	107.775 (2)	93.6350 (10)	93.2680 (10)	92.792 (6)	92.149 (2)		91.416 (8)
V (Å^3)	1367.06 (12)	1351.73 (7)	1419.28 (19)	1367.02 (15)	1446.79 (18)	1403.9 (5)	1519.6 (2)	909.28 (7)	931.0 (5)
R_1	0.030	0.020	0.030	0.029	0.017	0.030	0.025	0.019	0.042
Reference	Siidra *et al.* (2018*b*)	Kovrugin *et al.* (2019)	Siidra *et al.* (2021*c*)	Borisov *et al.* (2021)	Zhou *et al.* (2020)	Siidra *et al.* (2021*b*)	Siidra *et al.* (2021*b*)	Siidra *et al.* (2021*b*)	This work

the ionic radius of the alkali metal cation(s), embedded in the $[Cu(SO_4)_2]^{2-}$ framework, symmetry-breaking transformations occur.

Comparative topological analysis of known $A_2Cu(SO_4)_2$ phases (Table 5) revealed some common building units, which represent the 2,4C4 chains according to the *ToposPro* TTD nomenclature (Blatov *et al.*, 2021), where the numbers 2 and 4 are equal to the coordination numbers of sulfate groups and copper atoms in the underlying net, letter C designates a chain (1-periodic) underlying net, and the last number (4) enumerates topologically different nets with the same 2,4C signature (Fig. 8). The structures of α, β and γ forms are assembled from these chains by sharing apical oxygens of the CuO_5 tetragonal pyramids of one chain with sulfate anion of another chain. Increasing size requirements and decreasing polarizing activity of alkali cations occupying the space between chains result in different packing and connectivity of the chains which provide the different topologies. In the δ- and ε-phases, the quadrangular $Cu_2(SO_4)_2$ rings of the chains are broken and the 'dangling' links participate in additional contacts between the groups (Fig. 7).

The coordination environments of the Cu^{2+} sites demonstrate significant changes in the saranchinaite morphotropic series. There are four symmetry-independent Cu sites in saranchinaite $Na_2Cu(SO_4)_2$ (Siidra *et al.*, 2018*b*) and its synthetic analog (Kovrugin *et al.*, 2019). The environments of Cu1 and Cu4 atoms are similar, thus coordination of Cu4 only is provided in Fig. 7. Each Cu atom in saranchinaite forms four short Cu–O_{eq} bonds ($\leq$2 Å) in CuO_4 squares complemented by a fifth, longer Cu—O_{ap} bond of ~2.3 Å, to form CuO_5 distorted tetragonal pyramids. There are also two essentially longer Cu—O_{add} bonds in the 2.9–3.1 Å range. Taking them into consideration, the overall coordination polyhedra of Cu^{2+} can be considered as 'octahedra with one split vertex'. Note, saranchinaite is the only representative wherein the Cu-centered (namely Cu2- and Cu3-centered) polyhedra are linked via a common oxygen vertex into dimeric units (Fig. 7). In addition to usual vertex corner sharing, each CuO_7 polyhedron shares two of its edges with the sulfate tetrahedra (Cu–S distance is ~3.0 Å). The alkali cations are embedded in several types of channel (large elliptical ones are marked in yellow in Fig. 7). Refinement of the crystal structure of the

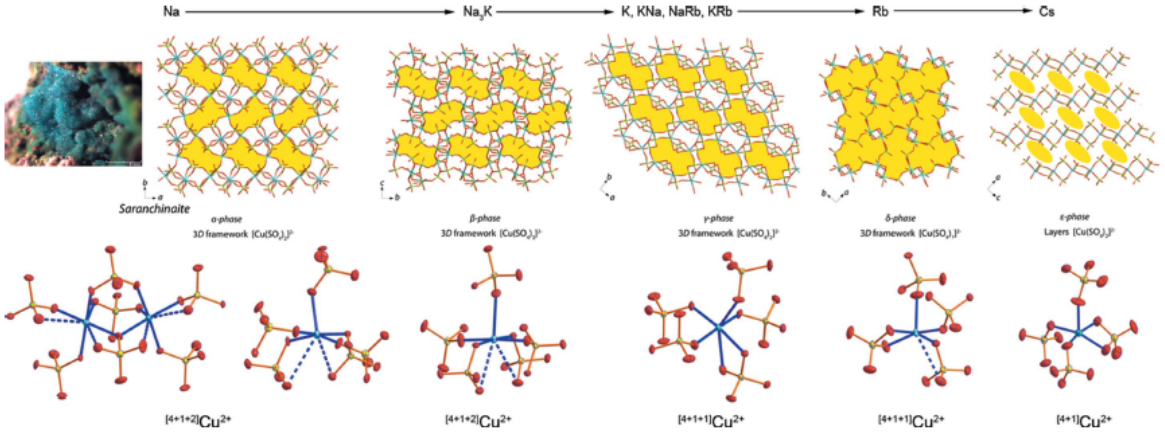

Figure 7
Evolution of $[Cu(SO_4)_2]^{2-}$ moieties in the structures of saranchinaite (in photo) morphotropic series $A_2Cu(SO_4)_2$ (A = Na, K, Rb, Cs) compounds. Elliptical channels are marked in yellow (upper row). Coordination of CuO_n polyhedra by SO_4 groups in each phase (lower row). Distances in Å. Cu—O bonds >2.6 Å are shown by blue dotted lines. See the text for details.

mineral (Siidra *et al.*, 2018*b*) shows the presence of the minor potassium admixture ($Na_{0.7}K_{0.3}$) in one of eight symmetry-independent alkali sites.

Cu-centered dimers are disintegrated into isolated CuO_7 polyhedra in the structure of $K(Na,K)Na_2[Cu_2(SO_4)_4]$, a hitherto unique representative of the β form (Siidra *et al.*, 2021*c*). Apart from this difference, no other significant changes in the coordination of the divalent copper cation from the mineral described above are observed. There are two symmetry-independent copper sites in $K(Na,K)Na_2[Cu_2(SO_4)_4]$, both with very similar coordination environments ($Cu1O_7$ is represented in Fig. 7). The overall structural topology of $[Cu(SO_4)_2]$ framework (Fig. 7) is significantly different from that in saranchinaite. Hence, the increase of the Na:K ratio to ~3:1 results in a complete rearrangement of the $[Cu(SO_4)_2]^{2-}$ moiety.

Further increase of the Na:K ratio to ~1:1 in $KNaCu(SO_4)_2$ (γ-phase) (Borisov *et al.*, 2021) results in significant changes in both Cu^{2+} coordination environments and the overall topology of the framework. Four Cu—O bonds with distances around 2 Å form a nearly square planar configuration, the bond with a fifth O atom is somewhat longer (~2.2 Å) and its orientation is almost perpendicular to the square plane. There is an additional Cu—O bond of 2.6 Å strongly bent away from 180° which would be expected for an 'ideal' [4+1+1] octahedron. The CuO_6 polyhedron shares one of its edges with an SO_4 tetrahedron with the Cu–S distance of 2.8 Å in $KNaCu(SO_4)_2$ (Borisov *et al.*, 2021). The same structure type is adopted by $K_2[Cu(SO_4)_2]$ (Zhou *et al.*, 2020), $RbNa[Cu(SO_4)_2]$ and $RbK[Cu(SO_4)_2]$ (Siidra *et al.*, 2021*a*) which illustrates a remarkable flexibility of this framework architecture (Table 5); note however that the 'single-alkali' potassium compound was obtained at low temperatures and

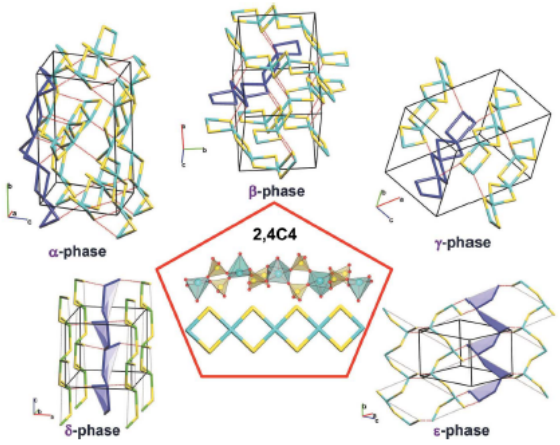

Figure 8
Assembling of $[Cu(SO_4)_2]^{2-}$ moieties in $A_2Cu(SO_4)_2$ phases from the 2,4C4 chains. Light-blue and yellow nodes of the underlying nets depict copper cations and sulfate anions, respectively. The links between the chains are shown by red dotted lines. One chain in each phase is highlighted in blue; in δ- and ε-phases the open $Cu_2(SO_4)_2$ rings in this chain are shaded.

Table 6
Crystallographic parameters of orthorhombic $A_2M^{2+}{}_2(SO_4)_3$ compounds.

Formula	$K_2Cu_2(SO_4)_3$	$Rb_2Cu_2(SO_4)_3$	$Cs_2Co_2(SO_4)_3$
Space group	$P2_12_12_1$	$P2_12_12_1$	$P2_12_12_1$
a (Å)	4.81065 (1)	4.8359 (19)	4.8810 (7)
b (Å)	11.91795 (3)	12.294 (4)	14.920 (2)
c (Å)	18.67516 (4)	19.036 (7)	17.164 (3)
V (Å)^3	1070.704 (4)	1131.7 (7)	1249.9 (3)
R_1	0.048	0.052	0.049
Reference	Lander *et al.* (2017)	Siidra *et al.* (2021*b*)	This work

something quite different is produced in a traditional ceramic synthesis, according to the unindexed ICDD card 17-0485. Also, the essential size differences, *e.g.* between Rb^+ and Na^+ in the structure of $RbNa[Cu(SO_4)_2]$, can be somewhat 'smeared' by mixed occupancies of cationic sites.

The other 'single-alkali' member, $Rb_2[Cu(SO_4)_2]$ [δ-phase; Siidra *et al.* (2021*a*)] crystallizes in space group $Pna2_1$ (Table 5). Only large elliptical channels remain in $[Cu(SO_4)_2]^{2-}$ open framework (Fig. 7). One symmetry-independent Cu atom forms a CuO_5 distorted tetragonal pyramid with an $Cu—O_{ap}$ bond of 2.182 (1) Å. One additional long Cu—O bond of 2.994 (4) Å results in a strongly distorted [4+1+1] CuO_6 octahedron. Two of the O–O octahedron edges are shared with κ^2-coordinated SO_4 tetrahedra (with corresponding Cu–S distances of 2.6 and 3.0 Å).

Finally, $Cs_2[Cu(SO_4)_2]$, which we designate as the ε-phase, has a layered character. The coordination of Cu^{2+} by sulfate groups to form CuO_5 polyhedra is described above in detail.

The observed trend of gradual decrease of Cu coordination number with increasing size of the A^+ ionic radius, which defines the crystal chemical boundaries of the polymorphs, is an interesting manifestation of fine chemical tuning. A similar phenomenon has been recently observed in the family of $(AX)[Cu(HSeO_3)_2]$ (A = Na, K, NH_4, Rb, Cs; X = Cl, Br) compounds (Charkin *et al.*, 2019) wherein fine structural details of Cu^{2+} coordination within the $[Cu(HSeO_3)_2]$ slabs were also dependent on the size of the univalent cation. Determination of the structural architectures of anhydrous

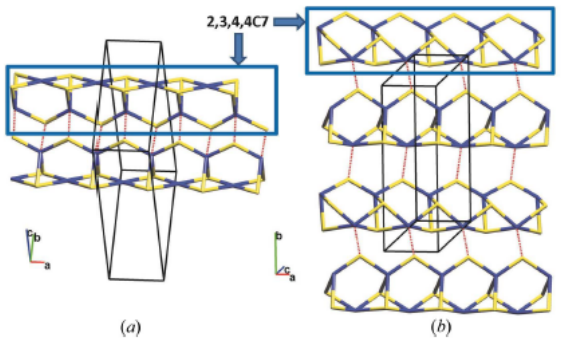

Figure 9
Assembling of $[M^{2+}{}_2(SO_4)_3]^{2-}$ moieties in $A_2M^{2+}{}_2(SO_4)_3$ phases from the 2,3,4,4C7 chains. Blue and yellow nodes of the underlying nets depict M^{2+} cations and sulfate anions, respectively. The links between the chains are shown by red dotted lines.

sulfates in saranchinaite morphotropic series should be useful in phase identification and decomposition products of hydrated alkali transition metal sulfates $A^{+}{}_2M^{2+}(SO_4)_2{\cdot}nH_2O$ (*e.g.* Majzlan *et al.*, 2021) with various possible and existing applications.

4.2. $Cs_2Co_2(SO_4)_3$

As in the previous case, only two hydrated species, $Cs_2Co(SO_4)_2{\cdot}6H_2O$ (Tutton salt; Kockelmann *et al.*, 2001) and $CsCo(SO_4)_2{\cdot}12H_2O$ (Co^{3+}-based alum; Beattie *et al.*, 1981) were known prior to our work, whereas anhydrous species remained unreported.

$Cs_2Co_2(SO_4)_3$ is a new representative of another morphotropic series of the orthorhombic $A_2M^{2+}{}_2(SO_4)_3$ family (Table 6). To date, attempts aimed at preparation of $Cs_2Cu_2(SO_4)_3$ were not successful which might probably indicate that this composition may lie beyond the stability limit for this architecture. Similar to previously described $K_2Cu_2(SO_4)_3$ (Lander *et al.*, 2017) and $Rb_2Cu_2(SO_4)_3$ (Siidra *et al.*, 2021*a*), $Cs_2Co_2(SO_4)_3$ also adopts space group $P2_12_12_1$. Unit-cell metrics are also similar with *a* parameter value almost the same in all three representatives known to date. However, while the anionic part in the isostructural Cu compounds is characterized by one-dimensional chains, the $[Co_2(SO_4)_3]^{2-}$ architecture in $Cs_2Co_2(SO_4)_3$ is layered. It is not clear yet whether Cs^{+} or Co^{2+} or both define this morphotropic boundary, while it is clearly the cation size which demarcates the orthorhombic $Cs_2Co_2(SO_4)_3$ structure from the cubic langbeinites $K_2Co_2(SO_4)_3$ (Speer & Salje, 1986), $Tl_2Co_2(SO_4)_3$ (ICDD Card No. 22-1466) and $Rb_2Co_2(SO_4)_3$ (ICDD Card No. 22-1266). It is thus of interest to see whether similar or different structures and relationships would be observed for other $Cs_2M^{II}{}_2(SO_4)_3$ compounds whereof only the Co compound reported here is currently known.

The orthorhombic $A_2M^{2+}{}_2(SO_4)_3$ phases form the underlying nets wherein the M^{2+} cations and sulfate anions have the same coordination numbers, which is reflected by similar *ToposPro* TTD symbols 3,3,4,5C21 (*A* = K, Rb) and 3,3,4,5L54 (*A* = Cs). The difference in the periodicity of the underlying nets is shown in the symbols by letters C (chain) and L (layer). The coordination similarity suggests a topological interrelation between these two topologies. Indeed, both chain and layer units can be assembled from the same $[M^{2+}{}_2(SO_4)_3]^{2-}$ bands of the 2,3,4,4C7 topology (Fig. 9). The difference is that in the potassium- and rubidium-containing phases the 2,3,4,4C7 chains are assembled in pairs thus forming the 3,3,4,5C21 bands, while in $Cs_2Co_2(SO_4)_3$ the same number of the links interconnects a chain with the two other chains thus forming a layer (Fig. 9).

5. Implications and outlook

Among other features, the structures reported here reflect the variability and relative flexibility of coordination sphere of not only copper, but also of cobalt. The preferences of transition metal dications to adopt octahedral coordination are in line with the values of the respective crystal field stabilization energy (CSFE) and Jahn–Teller effect. For Cu^{2+} ($3d^9$), the CSFE is low ($^1/_5\Delta_o$) and the JT effect is strong which explains the utmost 'plasticity' of its coordination sphere. A similar pattern is observed for Zn^{2+} ($3d^{10}$) and sometimes Mg^{2+} (non-transition element) with CSFE = 0. The octahedral coordination is more common for high-spin Co^{2+} ($3d^7$, CSFE = $\frac{4}{5}\Delta_o$), yet environments different from octahedral are also possible. Among anhydrous sulfates and oxide sulfates, Zn^{2+} and Cu^{2+} easily substitute for each other (Siidra *et al.*, 2018*a*); there is one example from the chemistry of structurally related molybdates (Reichelt *et al.*, 2005) illustrating essential effects of this substitution on the magnetic properties. Substitution of Co^{2+} for Zn^{2+} in ZnO also produced interesting magnetic effects (Rode *et al.*, 2008), to say nothing about the excellent color properties of the Rinmann's green-based $Zn_{1-x}Co_xO$ pigments. To date, the examples of Co^{2+} substituting for Cu^{2+} are reported mostly for the octahedral and tetrahedral environments typical for spinels and salt hydrates (*e.g.* Tutton salts). The chemistry of anhydrous (oxide) sulfates provides rare and specific opportunities for stabilizing less common environments for these magnetically active cations. It is also possible that in more complex mixed-cations Co^{2+} and Cu^{2+} would order to provide new uncommon crystal structures and magnetic behavior. Investigation of pseudo-binary and more complex sulfate systems are expected to shed more light into the crystal chemistry and magnetochemistry of these unusual families.

Acknowledgements

Technical support by the SPbSU Resource Centers is gratefully acknowledged.

Funding information

Funding for this research was provided by: Russian Foundation for Basic Research (grant No. 19-05-00413).

References

Ballirano, P., Belardi, G. & Bosi, F. (2007). *Acta Cryst.* E**63**, m165–m165.

Beattie, J. K., Best, S. P., Skelton, B. W. & White, A. H. (1981). *J. Chem. Soc. Dalton Trans.* pp. 2105–2111.

Blatov, V. A. (2006). *Acta Cryst.* A**62**, 356–364.

Blatov, V. A., Alexandrov, E. V. & Shevchenko, A. P. (2021). In *Comprehensive Coordination Chemistry III*, edited by E. C. Constable, G. Parkin, L. Que Jr, pp. 389–412. Elsevier.

Blatov, V. A., Shevchenko, A. P. & Proserpio, D. M. (2014). *Cryst. Growth Des.* **14**, 3576–3586.

Borisov, A. S., Siidra, O. I., Kovrugin, V. M., Golov, A. A., Depmeier, W., Nazarchuk, E. V. & Holzheid, A. (2021). *J. Appl. Cryst.* **54**, 237–250.

Bruker-AXS (2014). *APEX2*, Version 2014.11-0. Bruker-AXS, Madison, Wisconsin, USA.

Burns, P. C. & Hawthorne, F. C. (1995). *Can. Mineral.* **33**, 889–905.

Charkin, D. O., Markovski, M. R., Siidra, O. I., Nekrasova, D. O. & Grishaev, V. Yu. (2019). *Z. Kristallogr. Cryst. Mater.* **234**, 739–747.

Filatov, S. K., Shablinskii, A. P., Krivovichev, S. V., Vergasova, L. P. & Moskaleva, S. (2020). *Mineral. Mag.* **84**, 691–698.

Foret, F., Langfelderová, H. & Gažo, J. (1982). *J. Therm. Anal.* **25**, 487–498.

Gagné, O. C. & Hawthorne, F. C. (2015). *Acta Cryst.* B**71**, 562–578.

Giacovazzo, C., Scandale, E. & Scordari, F. (1976). *Z. Kristallogr.* **144**, 226–237.

Hawthorne, F. C., Krivovichev, S. V. & Burns, P. C. (2000). *Rev. Miner. Geochem.* **40**, 1–112.

Kockelmann, W., Schäfer, W., Kirfel, A., Klapper, H. & Euler, H. (2001). *Mater. Sci. Forum*, **378–381**, 274–281.

Kovrugin, V. M., Nekrasova, D. O., Siidra, O. I., Mentré, O., Masquelier, C., Stefanovich, S. Yu. & Colmont, M. (2019). *Cryst. Growth Des.* **19**, 1233–1244.

Lander, L., Rousse, G., Batuk, D., Colin, C. V., Dalla Corte, D. A. & Tarascon, J.-M. (2017). *Inorg. Chem.* **56**, 2013–2021.

Majzlan, J., Marinova, D. & Dachs, E. (2021). *RSC Adv.* **11**, 374–379.

Marsh, R. E. (1995). *Acta Cryst.* B**51**, 897–907.

Nagase, K., Yokobayashi, H. & Sone, K. (1978). *Thermochim. Acta*, **23**, 283–291.

Nekrasova, D. O., Siidra, O. I., Zaitsev, A. N., Ugolkov, V. L., Colmont, M., Charkin, D. O., Mentré, O., Chen, R., Kovrugin, V. M. & Borisov, A. S. (2021*a*). *Phys. Chem. Miner.* **48**, 6.

Nekrasova, D. O., Tsirlin, A. A., Colmont, M., Siidra, O. I., Vezin, H. & Mentré, O. (2020). *Phys. Rev. B*, **102**, 184405.

Nekrasova, D. O., Tsirlin, A., Colmont, M., Siidra, O., Arevalo-Lopez, A. & Mentré, O. (2021*b*). *Inorg. Chem.* **60**, 18185–18191.

Papánková, B., Langfelderová, H., Sivý, P. & Serátor, M. (1985). *Z. Anorg. Allg. Chem.* **526**, 203–208.

Pekov, I. V., Zubkova, N. V., Agakhanov, A. A., Pushcharovsky, D. Yu., Yapaskurt, V. O., Belakovskiy, D. I., Vigasina, M. F., Sidorov, E. G. & Britvin, S. N. (2018). *Eur. J. Mineral.* **30**, 593–607.

Reichelt, W., Steiner, U., Söhnel, T., Oeckler, O., Duppel, V. & Kienle, L. (2005). *Z. Anorg. Allg. Chem.* **631**, 596–603.

Rode, K., Mattana, R., Anane, A., Cros, V., Jacquet, E., Contour, J.-P., Petroff, F., Fert, A., Arrio, M., Sainctavit, P., Bencok, P., Wilhelm, F., Brookes, N. B. & Rogalev, A. (2008). *Appl. Phys. Lett.* **92**, 012509.

Sheldrick, G. M. (2015). *Acta Cryst.* A**71**, 3–8.

Siidra, O. I., Borisov, A. S., Charkin, D. O., Depmeier, W. & Platonova, N. V. (2021*a*). *Mineral. Mag.* **85**, 262–277.

Siidra, O. I., Charkin, D. O., Kovrugin, V. M. & Borisov, A. S. (2021*c*). *Acta Cryst.* B**77**, 1003–1011.

Siidra, O. I., Lukina, E. A., Nazarchuk, E. V., Depmeier, W., Bubnova, R. S., Agakhanov, A. A., Avdontseva, E. Yu., Filatov, S. K. & Kovrugin, V. M. (2018*b*). *Mineral. Mag.* **82**, 257–274.

Siidra, O. I., Nazarchuk, E. V., Agakhanov, A. A., Lukina, E. A., Zaitsev, A. N., Turner, R., Filatov, S. K., Pekov, I. V., Karpov, G. A. & Yapaskurt, V. O. (2018*a*). *Mineral. Petrol.* **112**, 123–134.

Siidra, O. I., Nazarchuk, E. V., Zaitsev, A. N., Lukina, E. A., Avdontseva, E. Y., Vergasova, L. P., Vlasenko, N. S., Filatov, S. K., Turner, R. & Karpov, G. A. (2017). *Eur. J. Mineral.* **29**, 499–510.

Siidra, O. I., Nazarchuk, E. V., Zaitsev, A. N. & Shilovskikh, V. V. (2020). *Mineral. Mag.* **84**, 153–158.

Siidra, O. I., Nekrasova, D. O., Charkin, D. O., Zaitsev, A. N., Borisov, A. S., Colmont, M., Mentré, O. & Spiridonova, D. V. (2021*b*). *Mineral. Mag.* **85**, 813–845.

Speer, D. & Salje, E. (1986). *Phys. Chem. Miner.* **13**, 17–24.

Tardy, M., Bregeault, J.-M. & Pannetier, G. (1972). *Bull. Soc. Chim. Fr.* pp. 2658–2662.

Testasicca, L. P., Frost, R. L., Ruan, X., Lima, J., Belotti, F. M. & Scholz, R. (2016). *J. Therm. Anal. Calorim.* **126**, 1089–1095.

Vergasova, L. P. & Filatov, S. K. (2012). *J. Volcanol. Seismol.* **6**, 281–289.

Zubkova, N. V., Pekov, I. V., Agakhanov, A. A., Ksenofontov, D. A. & Pushcharovsky, D. Yu. (2021). *Crystallogr. Rep.* **66**, 60–65.

Zhou, H. A., Liu, Z., Ang, S. S. & Zhang, J.-J. (2020). *Solid State Sci.* **100**, 106104.